ISSN 1674-1056
http://cpb.iphy.ac.cn
http://iopscience.iop.org/cpb
中国物理 B
Chinese Physics
中国物理
Chinese Physics B

Direct observation of melted Mott state evidenced from Raman scattering in 1 *T*-TaS_2 single crystal

Qing Hu(胡庆), Cong Yin(尹聪), Leilei Zhang(张雷雷), Li Lei(雷力), Zhengshang Wang(王正上), Zhiyu Chen(陈志禹), Jun Tang(唐军), Ran Ang(昂然)
Citation: Chin. Phys. B . 2018, 27(1): 017104. **doi:** 10.1088/1674-1056/27/1/017104

Journal homepage: http://cpb.iphy.ac.cn; http://iopscience.iop.org/cpb

What follows is a list of articles you may be interested in

Recent progress on integrating two-dimensional materials with ferroelectrics for memory devices and photodetectors

Jianlu Wang(王建禄), Weida Hu(胡伟达)
Chin. Phys. B . 2017, 26(3): 037106. **doi:** 10.1088/1674-1056/26/3/037106

Identification of surface oxygen vacancy-related phonon-plasmon coupling in TiO_2 single crystal

Jun-Hong Guo(郭俊宏), Ting-Hui Li(李廷会), Fang-Ren Hu(胡芳仁), Li-Zhe Liu(刘力哲)
Chin. Phys. B . 2016, 25(12): 127103. **doi:** 10.1088/1674-1056/25/12/127103

Homopolar bonds in Se-rich Ge—As—Se chalcogenide glasses

Si-Wei Xu(许思维), Rong-Ping Wang(王荣平), Zhi-Yong Yang(杨志勇), Li Wang(王丽), Luther-Davies Barry
Chin. Phys. B . 2016, 25(5): 057105. **doi:** 10.1088/1674-1056/25/5/057105

Effect of 6H-SiC (1120) substrate on epitaxial graphene revealed by Raman scattering

Lin Jing-Jing, Guo Li-Wei, Jia Yu-Ping, Chen Lian-Lian, Lu Wei, Huang Jiao, Chen Xiao-Long
Chin. Phys. B . 2013, 22(1): 016301. **doi:** 10.1088/1674-1056/22/1/016301

High sensitivity refractive index gas sensing enhanced by surface plasmon resonance with nano-cavity antenna array

Zhao Hua-Jun
Chin. Phys. B . 2012, 21(8): 087104. **doi:** 10.1088/1674-1056/21/8/087104

RAPID COMMUNICATION

Direct observation of melted Mott state evidenced from Raman scattering in 1T-TaS_2 single crystal*

Qing Hu(胡庆)[1,#], Cong Yin(尹聪)[1,#], Leilei Zhang(张雷雷)[2], Li Lei(雷力)[2,‡], Zhengshang Wang(王正上)[1], Zhiyu Chen(陈志禹)[1], Jun Tang(唐军)[1,3], and Ran Ang(昂然)[1,3,†]

[1] *Key Laboratory of Radiation Physics and Technology, Ministry of Education, Institute of Nuclear Science and Technology, Sichuan University, Chengdu* 610064, *China*

[2] *Key Laboratory of High Energy Density Physics and Technology, Ministry of Education, Institute of Atomic and Molecular Physics, Sichuan University, Chengdu* 610065, *China*

[3] *Institute of New Energy and Low-Carbon Technology, Sichuan University, Chengdu* 610065, *China*

(Received 2 November 2017; revised manuscript received 9 November 2017; published online 1 December 2017)

The evolution of electron correlation and charge density wave (CDW) in 1T-TaS_2 single crystal has been investigated by temperature-dependent Raman scattering, which undergoes two obvious peaks of A_{1g} modes about 70.8 cm^{-1} and 78.7 cm^{-1} at 80 K, respectively. The former peak at 70.8 cm^{-1} is accordant with the lower Hubbard band, resulting in the electron-correlation-driven Mott transition. Strikingly, the latter peak at 78.7 cm^{-1} shifts toward low energy with increasing the temperature, demonstrating the occurrence of nearly commensurate CDW phase (melted Mott phase). In this case, phonon transmission could be strongly coupled to commensurate CDW lattice via Coulomb interaction, which likely induces appearance of hexagonal domains suspended in an interdomain phase, composing the melted Mott phase characterized by a shallow electron pocket. Combining electronic structure, atomic structure, transport properties with Raman scattering, these findings provide a novel dimension in understanding the relationship between electronic correlation, charge order, and phonon dynamics.

Keywords: two-dimensional materials, charge density wave, Mott state, Raman scattering

PACS: 71.45.Lr, 71.30.+h, 63.22.−m, 74.25.nd **DOI:** 10.1088/1674-1056/27/1/017104

1. Introduction

Coexistence, competition, and collaboration of electron correlation with charge order or charge-density-wave (CDW) are a long-term unresolved issue in low dimensional physics. While the CDW order is well understood by the conventional Peierls mechanism in terms of Fermi-surface nesting due to electron–phonon coupling, electron correlation also plays a crucial role as well in some circumstances.[1–4] Layered transition-metal dichalcogenides (TMDs)[5–8] provide an ideal platform for investigating the interplay in that their intrinsic two-dimensional structure is susceptible to electronic instability. Among many TMDs, it has attracted much attention in 1T-TaS_2, where its CDW phases include nearly commensurate CDW (NCCDW) and commensurate CDW (CCDW) phases. Additionally, its CCDW phase is compatible to the Mott insulating phase because of the strong electron–phonon and electron–electron interactions.[9–13]

Current explanation of 1T-TaS_2 and its associated phases, which is focused mainly on electronic states, can be summarized in four aspects: (i) Ta atoms are displaced to form star-of-David clusters where 12 Ta atoms contract toward a central Ta atom, interlocking each cluster to form a triangular superlattice.[9,10,14] However, the 12 electrons dominate the states below the distortion-induced gap and the thirteenth one occupies the states above the gap, leading to a Mott insulating state which is responsible for high resistivity of the CCDW phase.[15–17] (ii) The neighbouring NCCDW phase contains the star-of-David clusters, although they are less uniformly arranged.[9] (iii) Upon increasing temperature, the Mott phase melts into the NCCDW phase (the melted Mott phase) with an extremely fast charge response and a sudden resistivity drop, where several tens of stars organize into roughly hexagonal domains.[12,18] These reproduce locally the CCDW Mott phase, revealing that the CCDW mechanism is beyond the framework of the conventional Peierls picture.[19–22] (iv) The CCDW superlattice structure could be described by the trigonal structure due to the weak interlayer interaction.[23,24] Definitely, none of them have verified a seemly counter-intuitive origin in understanding the low-dimensional electron system.

In this work, we provide definitive evidence that electron-correlation-driven Mott transition and NCCDW transition

*Project supported by the National Natural Science Foundation of China (Grant Nos. 51771126 and 11774247), the Youth Foundation of Science and Technology Department of Sichuan Province, China (Grant No. 2016JQ0051), and the World First-Class University Construction Funding.

#These authors contributed equally to this work.

†Corresponding author. E-mail: rang@scu.edu.cn

‡Corresponding author. E-mail: lei@scu.edu.cn

© 2018 Chinese Physical Society and IOP Publishing Ltd

(melted Mott transition) can be directly confirmed by Raman scattering in 1T-TaS_2. The observed melted Mott phase reflected by a shallow electron pocket, i.e., likely hexagonal domains which pinned in an interdomain phase, could originate from strong coupling between phonon excitation and CCDW lattice. Combining the microstructure, transport properties, electronic structure with Raman scattering, the findings presented here may provide insight into approaches for manipulating various CDW phases to understand underlying physics in low-dimensional electron systems.

2. Experimental procedure

High-quality single crystals of 1T-TaS_2 was grown by the chemical vapor transport technique with iodine as a transport agent. The temperature dependence of resistivity and Seebeck coefficient were carried out using a standard four-probe configuration in a quantum design physical properties measurement system (PPMS). Thin-foil specimens for transmission electron microscopy (TEM) and scanning TEM (STEM) imaging were prepared by cutting single crystal from [0001] (c axis). The selected-area diffraction pattern (SADP) and TEM images were taken using the JEOL JEM-2010 F electron microscope operated at 200 kV. The high-angle annular dark-field (HAADF) and annular bright-field (ABF) images were taken with a 200-kV ARM-200FC STEM equipped with a probe corrector (CEOS Gmbh). Raman scattering spectra were recorded through a custom-built Raman system using a triple grating monochromator (Andor Shamrock SR-303i-B, EU) with an attached electron-multiplying CCD (ANDOR Newton DU970P-U VB, EU) excited with a 532 nm solid-state laser (RGB laser system, Germany). Low-temperature Raman experiments were performed with the Freezing Stage (THMS600, UK). Angle-resolved photoemission spectroscopy (ARPES) measurements were performed using a VG-SCIENTA SES2002 spectrometer with a high-flux He discharge lamp. The He–Iα ($h\nu = 21.218$ eV) resonance line was used to excite photoelectrons.

3. Experimental results and discussion

Figure 1(a) shows sketches of its crystal structure and atomic planes in 1T-TaS_2, in which the central Ta is octahedrally coordinated by six S atoms within the P-3m1 space group. One plane of the hexagonally arranged Ta atoms is sandwiched in between two planes of the hexagonally packed S atoms by weak van der Waals interactions, while they are covalently bonded within the TMD sheets.[9] Figure 1(b) shows each cluster interlocked by forming a triangular superlattice with a $\sqrt{13} \times \sqrt{13}$ periodicity.[9,10,14] The temperature dependence of in-plane resistivity ρ_{ab} is shown in Fig. 1(c). A first-order transition from the NCCDW to the CCDW phase is discovered below 200 K. To shed light on the species of carriers, thermoelectric power S as a function of temperature is presented as shown in Fig. 1(d). The transition of S follows the one from NCCDW to CCDW phase, in agreement with the transition of resistivity. Interestingly, the sign of S is altered and switches from negative to positive in the vicinity of the

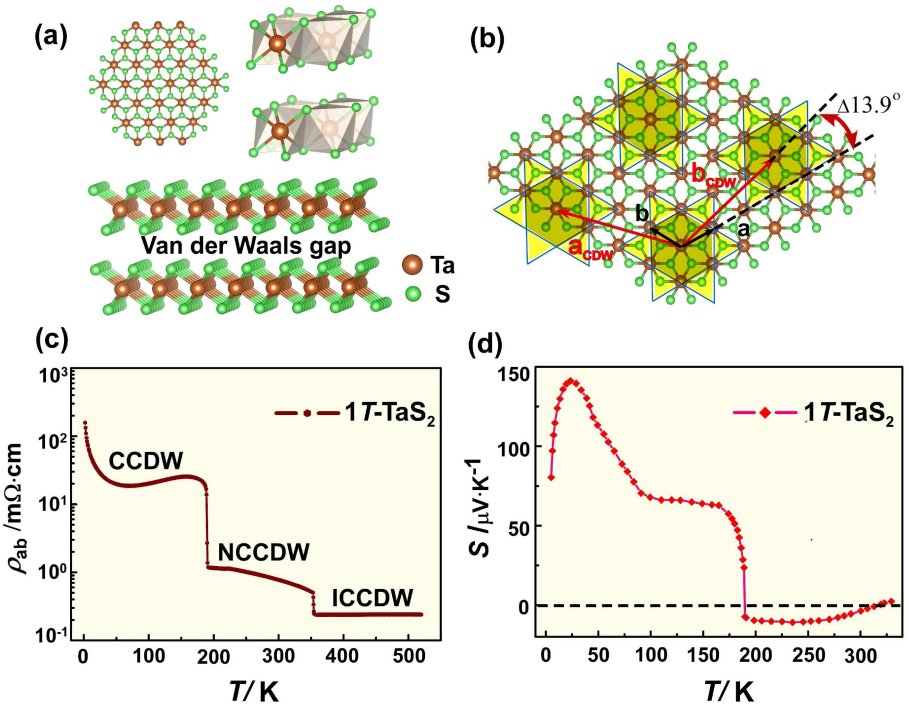


Fig. 1. (color online) (a) Crystal structure of 1T-TaS_2. (b) Commensurate CDW (CCDW) $\sqrt{13} \times \sqrt{13}$ triangular superlattice. The black and red arrows indicate the lattice vectors of 1×1 and $\sqrt{13} \times \sqrt{13}$ superstructure, respectively. (c), (d) Temperature dependence of in-plane resistivity (ρ_{ab}) and thermoelectric power S, respectively.

transition, indicating that the charge carriers change from electron type (n-type) to hole type (p-type). Below the temperature of NCCDW transition, more hole carriers dominate the transport properties, which exhibits large Seebeck coefficient at low temperatures.

To examine the microstructure of 1T-TaS_2, we performed TEM and SADP observed from [0001] orientation as shown in Figs. 2(a) and 2(b). The atomically thin flake of 1T-TaS_2 displays a uniform and smooth surface. The SADP with six-fold rotational symmetry confirms the hexagonal structure of 1T-TaS_2. In order to obtain high-resolution atomic structure further, the HAADF and ABF STEM viewed along c axis at room temperature have been indicated in Figs. 2(c) and 2(d). Since intensity of an atomic column in a HAADF imaging mode is proportional to $Z^{1.7}$ (Z is atomic number),[25] the brighter spots represent the Ta columns. Evidently, Ta atoms (marked by larger orange circles) are almost located at the identical sites in all cases, forming the star-of-David clusters, where stars are interlocked by forming a triangular superlattice with a $\sqrt{13} \times \sqrt{13}$ periodicity, in line with the crystal structure (see Figs. 1(a) and 1(b)). Surprisingly, only Ta atoms are visible in the HAADF image, whereas S atoms cannot be identified (Fig. 2(c)). Taking into account the fact that the much lighter S atoms are not scattered strongly enough to be visualized thus posing a significant hurdle to obtaining a complete structural configuration in terms of the HAADF STEM interpretation alone. To directly resolve all atomic columns, we take our newly developed ABF STEM imaging technique to observe 1T-TaS_2. The ABF STEM approach has been demonstrated

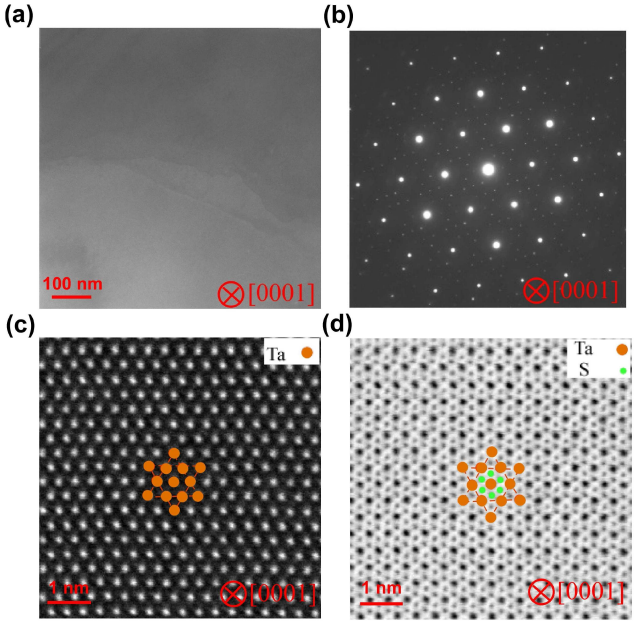


Fig. 2. (color online) (a) Low-resolution TEM image and (b) the corresponding SADP patters of 1T-TaS_2 along [0001] projection uncover the evident 6-fold rotational symmetry. (c) Atom-resolved HAADF and (d) ABF STEM images seen from [0001] projection (c axis). Brighter spots represent Ta atomic columns (larger orange circles), while darker ones S atomic columns (smaller green circles).

to allow a simultaneous imaging of light and heavy atoms with a good signal-to-noise ratio, robustly over a range of sample thickness.[26] Apart from conveying fundamental structural information as in the HAADF, the ABF STEM image, in which the dark spots represent atomic columns, identifies additional spots with weaker image contrast (smaller green circles) as the S columns (Fig. 2(d)), verifying the power of ABF technique.

To track the dynamical properties of lattice vibrations, we carried out Raman scattering measurements. There are two Raman-active phonon modes including A_{1g} and E_g modes,[27–29] in which A_{1g} mode refers to two S atoms per unit cell move relative to one another along z orientation, while a doubly-degenerate E_g mode reflects S atoms move opposite to one another along x or y orientation, as plotted in the inset of Fig. 3(a). Figure 3(b) shows the temperature-dependent Raman spectra of 1T-TaS_2. The modes with energies below 140 cm^{-1} as reflected by Fig. 3(c) should arise from acoustic phonon branches where vibration of Ta atoms dominates, while those above 220 cm^{-1} originate from optical branches where vibration of S atoms presides. It is found that 70.8, 78.7, 112.3, 127.0 cm^{-1} of the pronounced out-of-plane A_{1g} modes and 59.9, 88.4, 98.1 cm^{-1} of in-plane E_g modes are clearly observed at 80 K in the CCDW phase, defined as in Fig. 3(d). Especially for the two distinct peaks of $A_{1g}^{(1)}$ and $A_{1g}^{(2)}$ based on most remarkable intensity (i.e., 70.8 and 78.7 cm^{-1}), the $A_{1g}^{(1)}$ peak at 70.8 cm^{-1} is nearly temperature-independent in the CCDW phase and completely disappears above 160 K as plotted in Figs. 3(c) and 3(e). Such results reveal the Mott-Hubbard gap opening, which is triggered by enhancement of effective electron correlation.[11,16,22] The CCDW phase is composed of interlocking star-of-David (see Fig. 3(e)). The $A_{1g}^{(2)}$ peak at 78.7 cm^{-1} apparently shifts toward low energy as the temperature increases. The abrupt transition at $\sim$ 150 K demonstrates that the Mott phase melts into the NCCDW phase (the melted Mott phase) as plotted in Fig. 3(f), indicative of the NCCDW gap opening.[30,31] The melted Mott phase could be visualized as hexagonal domains suspended in an interdomain phase (see Fig. 3(f)).

To gain more insights into correlation between CCDW (Mott phase), NCCDW (melted Mott phase), electronic structure, and phonon transmission, we performed band dispersions based on ARPES along the ΓM cut measured at 30 K (Mott phase) and 300 K (melted Mott phase) as shown in Fig. 4(a). In the Mott phase at 30 K, the Ta 5d band splits into multiple subbands because of strong CDW potential. Also, near Fermi surface (E_F) spectral weight resides on the higher binding energy (E_B) side of $\sim$ 0.2 eV which originates from Mott transition and is assigned as the low Hubbard band (LHB).[17,32] In the NCCDW phase at 300 K, a highly dispersive band does not cross E_F but disperses back toward higher E_B near the

κ_F (Fermi vector) point, with a characteristic pseudogap (NCCDW gap) feature. Such band-folding behavior and ARPES-intensity modification are likely caused by the superlattice potential of the NCCDW where the star-of-David clusters locally maintain the $\sqrt{13} \times \sqrt{13}$ periodicity identical to the CCDW Mott phase. Inside the NCCDW gap, a narrow band pinned at E_F is also observed around the Γ point. Furthermore, the narrow band is verified as an intrinsic electron pocket across E_F.[31,33]

Figure 4(b) summarizes the band picture and phonon excitations in the CCDW and NCCDW phases, respectively. The shallow electron pocket appears in the NCCDW phase (melted Mott phase). This pocket is gapped in the Mott phase due to the enhanced electron correlation. In other words, the shallow electron pocket transforms into the LHB in the Mott phase further reveals an intimate link between the electron correlations, CCDW state, and NCCDW state. With increasing temperature, more phonons could be excited and coupled to CCDW lattice by Coulomb interaction, evidenced from observed Raman shift (see Fig. 3(f)). Therefore, the phonon propagation would result in corresponding fluctuations of CCDW state, which could cause the emergence of hexagonal domains suspended in the interdomain phase, forming the NCCDW state (melted Mott state) characterized by the shallow electron pocket (see Fig. 4(b)). The strongly coupled CCDW–phonon excitations would trigger large Raman intensity, in line with the experiment of Raman scattering (Figs. 3(b)–3(d)). The direct observation of charge-order transition from Raman scattering represents an important step forward in fully tailoring the CCDW phase (Mott insulating phase) and NCCDW phase.

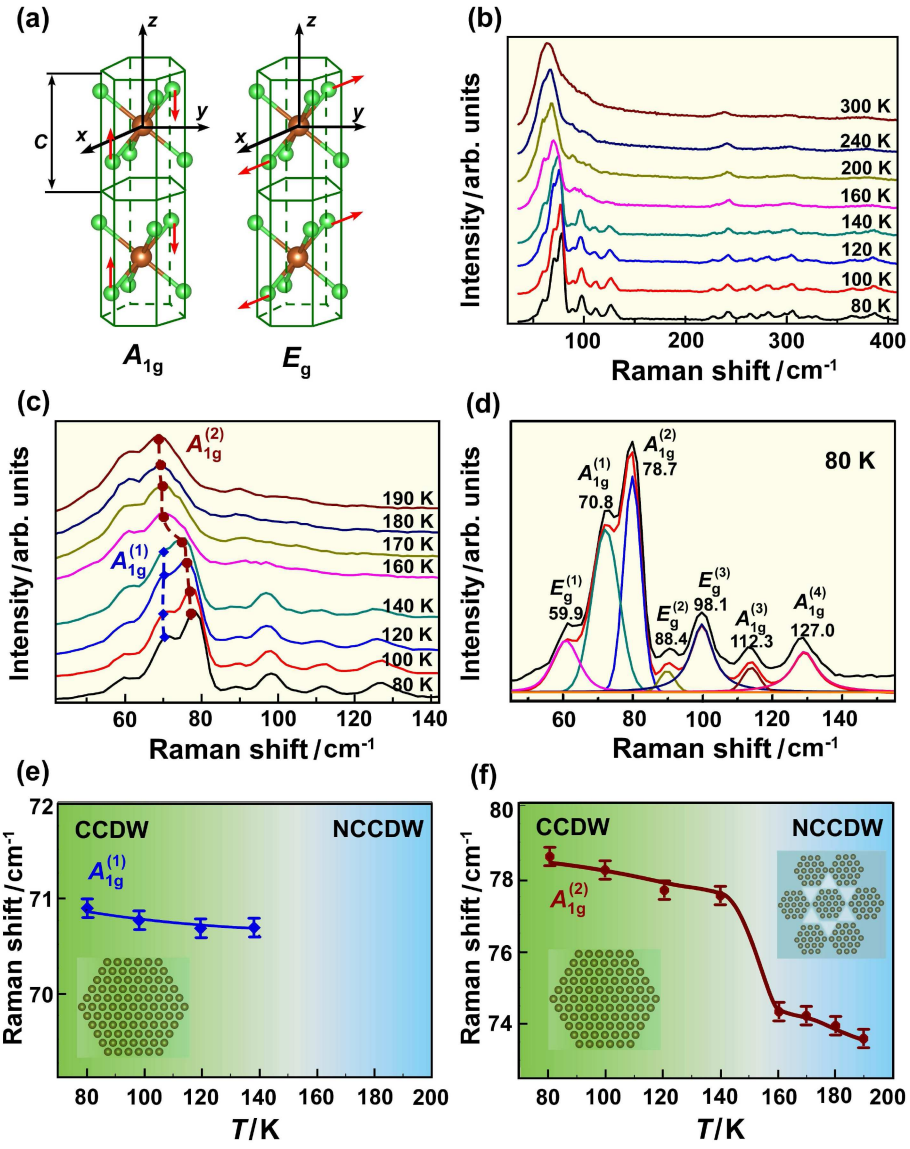


Fig. 3. (color online) (a) Two main types of crystal lattice Raman-active vibration A_{1g} and E_g modes in 1T-TaS_2. (b) Temperature-dependent Raman spectra in the cooling cycle from 300 to 80 K. (c) Temperature-dependent Raman spectra focused on the temperature range from 190 to 80 K. (d) All of fitting peaks derived from Raman spectra at 80 K. (e), (f) Shift of Raman peaks of $A_{1g}^{(1)}$ and $A_{1g}^{(2)}$ as a function of temperature, respectively. Evolution of superstructure illustrated from CCDW to NCCDW phase based on Raman spectra.

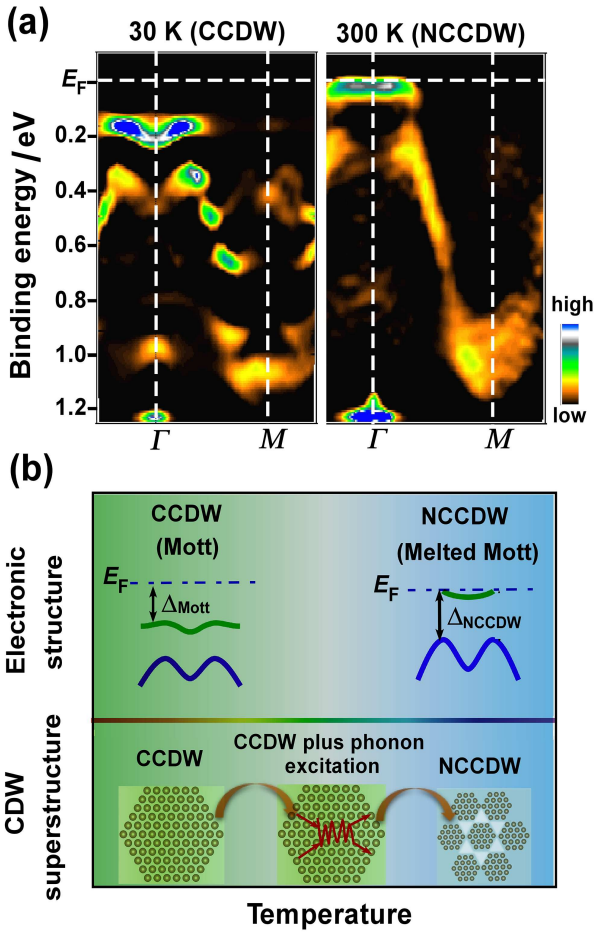


Fig. 4. (color online) (a) Second-derivative ARPES intensity of 1T-TaS_2 plotted as a function of wave vector and binding energy at 30 K and 300 K, respectively. (b) Schematic band diagram derived from the ARPES experiment and evolution of superstructure from CCDW to NCCDW phase before and after phonon excitation as a function of temperature.

4. Conclusion

We have reported the temperature dependence of Raman scattering in layered 1T-TaS_2 single crystal. We found direct evidence for electron-correlation-driven Mott transition and NCCDW transition (melted Mott transition) derived from Raman scattering. The electronic structure demonstrates that the shallow electron pocket is responsible for the melted Mott phase, where the possible hexagonal domains pinned in the interdomain phase, revealing strong coupling between phonon excitation and CCDW lattice. The present results not only render to recognize the intrinsic origin of Mott and NCCDW phases, but also provide a deep insight into close association between electronic correlation, charge-order state, and dynamical motions of phonons.

Acknowledgment

We thank Y. Liu, Y. P. Sun, Z. C. Wang, Y. Ikuhara, K. Nakayama, T. Sato, and T. Takahashi for the measurements of transport properties, atomic and electronic structures.

References

[1] Mathur N D, Grosche F M, Julian S R, Walker I R, Freye D M, Haselwimmer R K M and Lonzarich G G 1998 *Nature* **394** 39
[2] Lefebvre S, Wzietek P, Brown S, Bourbonnais C, Jérome D, Mézière C, Fourmigué M and Batail P 2000 *Phys. Rev. Lett.* **85** 5420
[3] Dagotto E 1994 *Rev. Mod. Phys.* **66** 763
[4] Damascelli A, Hussain Z and Shen Z X 1994 *Rev. Mod. Phys.* **75** 473
[5] Mattheiss L F 1973 *Phys. Rev. B* **8** 3719
[6] Gabovich A M, Voitenko A I and Ausloos M 2002 *Phys. Rep.* **367** 583
[7] Wang H T, Li L J, Ye D S, Cheng X H and Xu Z A 2007 *Chin. Phys. B* **16** 2471
[8] Yang H T, Tao H J and Zhang Z X 1998 *Chin. Phys. Lett.* **15** 123
[9] Wilson J A, Di Salvo F J and Mahajan S 1975 *Adv. Phys.* **24** 117
[10] Fazekas P and Tosatti E 1979 *Philos. Mag. B* **39** 229
[11] Manzke R, Buslaps T, Pfalzgraf B, Skibowski M and Anderson O 1989 *Europhys. Lett.* **8** 195
[12] Thomson R E, Burk B, Zettl A and Clarke J 1994 *Phys. Rev. B* **49** 16899
[13] Pillo T, Hayoz J, Berger H, Fasel R, Schlapbach L and Aebi P 2000 *Phys. Rev. B* **62** 4277
[14] Scruby C B, Williams P M and Parry G S 1975 *Philos. Mag.* **31** 255
[15] Rossnagel K and Smith N V 2006 *Phys. Rev. B* **73** 073106
[16] Smith N V, Kevan S D and Disalvo F J 1985 *J. Phys. C* **18** 3175
[17] Zwick F, Berger H, Vobornik I, Margaritondo G, Forró L, Beeli C, Onellion M, Panaccione G, Taleb-Ibrahimi A and Grioni M 1998 *Phys. Rev. Lett.* **81** 1058
[18] Spijkerman A, de Boer J L, Meetsma A, Wiegers G A and van Smaalen S 1997 *Phys. Rev. B* **56** 13757
[19] Hellmann S, Beye M, Sohrt C, Rohwer T, Sorgenfrei F, Redlin H, Kalläne M, Marczynski-Bühlow M, Hennies F, Bauer M, Föhlisch A, Kipp L, Wurth W and Rossnagel K 2010 *Phys. Rev. Lett.* **105** 187401
[20] Eichberger M, Schäfer H, Krumova M, Beyer M, Demsar J, Berger H, Moriena G, Sciani G and Miller R J D 2010 *Nature* **468** 799
[21] Ishizaka K, Kiss T, Yamamoto T, Ishida Y, Saitoh T, Matsunami M, Eguchi R, Ohtsuki T, Kosuge A, Kanai T, Nohara M, Takagi H, Watanabe S and Shin S 2011 *Phys. Rev. B* **83** 081104
[22] Petersen J C, Kaiser S, Dean N, Simoncig A, Liu H Y, Cavalieri A L, Cacho C, Turcu I C E, Springate E, Frassetto F, Poletto L, Dhesi S S, Berger H and Cavalleri A 2011 *Phys. Rev. Lett.* **107** 177402
[23] Sugai S, Murase K, Uchida S and Tanaka S 1981 *Physica B+C* **105** 405
[24] Duffey J R, Kirby R D and Coleman R V 1976 *Solid State Commun.* **20** 617
[25] Pennycook S J and Boatner L A 1988 *Nature* **336** 565
[26] Findlay S D, Shibata N, Sawada H, Okunishi E, Kondo Y, Yamamoto T and Ikuhara Y 2009 *Appl. Phys. Lett.* **95** 191913
[27] Uchida S and Sugai S 1981 *Physica B+C* **105** 393
[28] He R, Okamoto J, Ye Z P, Ye G H, Anderson H, Dai X, Wu X X, Hu J P, Liu Y, Lu W J, Sun Y P, Pasupathy A N and Tsen A W 2016 *Phys. Rev. B* **94** 201108
[29] Albertini O R, Zhao R, McCann R L, Feng S M, Terrones M, Freericks J K, Robinson J A and Liu A Y 2016 *Phys. Rev. B* **93** 214109
[30] Pillo Th, Hayoz J, Berger H, Grioni M, Schlapbach L and Aebi P 1999 *Phys. Rev. Lett.* **83** 3494
[31] Ang R, Tanaka Y, Ieki E, Nakayama K, Sato T, Li L J, Lu W J, Sun Y P and Takahashi T 2012 *Phys. Rev. Lett.* **109** 176403
[32] Perfetti L, Loukakos P A, Lisowski M, Bovensiepen U, Berger H, Biermann S, Cornaglia P S, Georges A and Wolf M 2006 *Phys. Rev. Lett.* **97** 067402
[33] Ang R, Miyata Y, Ieki E, Nakayama K, Sato T, Liu Y, Lu W J, Sun Y P and Takahashi T 2013 *Phys. Rev. B* **88** 115145